Development of an RTK-GPS system for precise real-time positioning of lightweight UAVs

Christian ELING, Lasse KLINGBEIL and Heiner KUHLMANN

1 Introduction

In recent years, micro- and mini-sized unmanned aerial vehicles (UAVs), which can be characterized having a weight limit of 5 kg and a size limit of 1.5 m (EISENBEIß 2009), have been used increasingly as mobile mapping platforms in remote sensing applications. Examples can be found in the fields of surveying, precision farming or infrastructure inspection. For these applications mostly a georeferencing of the collected data is required. This georeferencing can be done indirectly using ground control points (D'OLEIRE-OLTMANNS ET AL. 2012) or directly using an onboard sensor system (NAGAI ET AL. 2009). Since the indirect georeferencing is time-consuming and not real-time capable, the development of an onboard georeferencing system for UAVs is currently in great demand (BLÁHA ET AL. 2011). Direct georeferencing has extensively been researched in airborne applications (e.g. ŠKALOUD 1999). Thereby ordinarily DGPS/IMU systems are used. However, these systems cannot be adopted for micro- and mini-sized UAVs. There are two reasons for that: (1) Due to the lower flying altitude the GPS measurement conditions are often not ideal for UAV applications, especially, when the UAV flies next to buildings or trees. Therefore, additional sensors (e.g. IMU) play a more important role in the position and attitude determination of micro- and mini-sized UAVs. (2) The choice of the IMU is restricted by the space and the weight limitations of the UAV platform so that only a lower quality IMU can be used for the direct georeferencing. On this account further sensors (e.g. cameras) are needed to also allow for a reliable georeferencing during GPS losses of lock.

In this contribution a developed direct georeferencing system for lightweight UAVs is presented. This system is not only designed to enable a georeferencing of remote sensing data, but also to allow for an autonomous navigation of the UAV platform. For that purpose, the georeferencing needs to be processed in real-time and has to be robust. Generally, the georeferencing system is designed to have the following characteristics: (a) The weight of the system has to be less than 500 g so that the system is applicable on micro- and mini-sized UAVs. (b) The system has to be real-time capable. (c) Gaps of single sensors should be bridgeable by other sensors. (d) The system is intended to provide accurate positions (σ_{pos} < 5cm) and attitudes (σ_{att} < 1 deg). (e) The system is designed to allow for the integration of data from additional sensors, such as cameras or laserscanners.

A crucial part in the development of such a system is that the GPS processing algorithms of the system are in-house developed. There are different reasons for that:

(i) Especially in kinematic applications frequent losses of lock of the GPS signals occur (e.g. MORALES & TSUBOUCHI 2007). Since every loss of lock necessitates a re-initialization of the ambiguities, the ambiguity resolution has to be fast and robust at the same time for UAV applications. Furthermore, cycle slips in the carrier phases have to be detected and repaired reliably. Thus, the main reason for developing own GPS algorithms is to improve the ambiguity resolution and the cycle slip detection, which can for example be done in a

tightly-coupled approach, where the GPS observations are directly fused with the observations of additional sensors, such as inertial sensors or cameras.
(ii) In commercial software there is generally no access to the source code. Thus, expert users cannot gain an insight into the algorithms running in the background. Furthermore, adaptations according to special uses are generally impossible.
(iii) In the development of a real-time system the implemented software has to meet the requirements of the operating system that is running on the real-time unit. In this context also the task scheduling and the data management play an important role. Hence, the integration of a commercial software in such a system is often difficult or impossible. This also applies to the integration of open source software such as RTKLIB.

In the project presented in this paper the development and the implementation of tightly-coupled RTK-GPS and GPS attitude determination algorithms are aimed at. However, the development of these algorithms has not yet been completed. Nevertheless, as an intermediate state of this development, the basic concept of the RTK-GPS algorithm and the way how this algorithm is implemented on the onboard real-time processing unit will be discussed in this contribution. On this account, this contribution is mainly focused on the development of an RTK-GPS system for the positioning of micro- and mini-sized UAVs.
In section 2 the sensors, the setup of the developed direct georeferencing system as well as its integration into the UAV platform is explained. Afterwards, in section 3, details of the implemented RTK-GPS algorithm are presented. After a presentation of a field test (section 4) an outlook to the current and future work on the system will conclude this contribution (section 5).

2 The direct georeferencing system

2.1 Design of the direct georeferencing system

The main sensors of the georeferencing system are a geodetic grade dual-frequency GPS board (Novatel OEM 615), a MEMS IMU (Analog devices ADIS 16488) and a single frequency GPS chip (Ublox LEA6T). These sensors are directly connected to a real-time processing unit (National Instruments sbRIO 9606). This link is realized by an in-house designed 6-layer printed circuit board (PCB). The whole system is named the *PO*-board (position and orientation board).
In figure 1 a block diagram of the current version of the *PO*-board with the implemented interfaces is shown. The reason for choosing the sbRIO as processing unit is that it consists of a FPGA and a 400 MHz processor on one board so that the FPGA can be used to realize the interfaces to the onboard sensors and the 400 MHz processor can be used to compute the positions, velocities and attitudes of the UAV in real-time. The advantages of this combination are that (1) the FPGA is reconfigurable, with the result that all the software implemented interfaces can be modified easily, (2) the FPGA is very fast so that the decoding and preprocessing of the data from the different sensors can be realized in parallel and (3) the FPGA provides the data for the 400 MHz processor via direct memory accesses (DMAs) without a time delay.
To allow for the determination of RTK-GPS positions on the *PO*-board, the GPS raw observations from a master station have to be transmitted to the onboard system. The link to the GPS master station is realized by XBee Pro 868 long-range radio frequency modules.

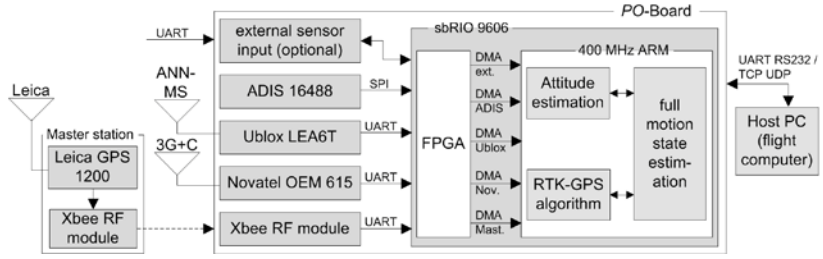

Fig. 1: The implemented interfaces and the data flow of the *PO*-board.

In addition to the RTK-GPS processing the observations from the Novatel receiver are also intended to be used for the attitude determination. For this purpose a second GPS receiver (LEA6T) is implemented on the *PO*-board and the two GPS antennas (NavExperience 3G+C, Ublox ANN-MS) form a short baseline on the UAV. The attitude determination is not in the focus of this paper. Summarizing, it is based on angular rates, accelerations and magnetic field observations from the IMU as well as on the onboard GPS baseline. The idea is that the angular rates, the accelerations and the magnetic field observations are first used to determine an approximate 3D attitude solution in a quaternion based extended Kalman filter. The accuracies of this solution are 1-5 deg, depending on the distortion of the calibrated magnetometer. Afterwards, the approximate attitude solution is used to fix the ambiguities of the single-frequency GPS baseline in a tightly-coupled approach (e.g. ELING ET AL. 2013b). Once the ambiguities could be fixed, the final attitude determination is accomplished fusing the angular rates, the accelerations and the GPS baseline.
Beside the named sensors also interfaces to optional external sensors, such as stereo camera systems or a laserscanner, are implemented. Via these interfaces information from visual or laser odometry algorithms can be integrated in the position and the attitude determination algorithms. In the current implementation the attitude and the RTK-GPS processing is realized in separated tasks. In the future, the final georeferencing will be performed by a superior filter task, where the GPS observations will just be one of many observation types.

The realization of the *PO*-board is shown in figure 2 (left). This unit is a redesigned version of the system presented in (ELING ET AL. 2013a). Together with both GPS antennas the total price of the direct georeferencing system is approximately 13000 €, from which the Novatel OEM 615 has a share of 8900 €. The weight of the unit is approximately 390 g. In order to reduce the weight as much as possible, the dual-frequency antenna (3G+C) was dismantled with the result that the weight could be reduced from 350 g to 100 g (see figure 2, right). Since the antenna reference point got lost in this process, the antenna had to be recalibrated in an anechoic chamber for further use (ZEIMETZ & KUHLMANN 2010). By comparison to the original antenna, the dismantling led to significant changes in the phase center offset (ca. 4 cm in the Up, < 1 mm in the North and the East component) and in the phase center variations (< 5 mm) of the antenna.

2.2 Software development

Generally, the programming of the FPGA and the 400 MHz processor is done using LabView™, which is a visual programming language from National Instruments™. The reason for choosing LabView™ is that this programming language is well suited for the development and administration of parallel real time tasks. Since the system is always in motion

and short latencies may lead to distinct position and attitude errors, the time-deterministic processing is very important in this development. Therefore, the operating system that is running on the 400 MHz processor is a RTOS (real-time operating system).
The RTK-GPS and the attitude determination algorithms are written in C++. The import of this software into the visual programming environment of LabView™ was realized by single dynamic link libraries (.dll-files), which are then called by the different RTOS tasks.

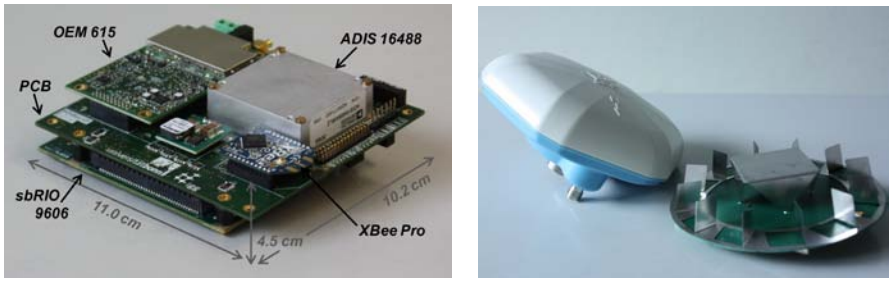

Fig. 2: The *PO*-board seen from the top-view (left) and comparison of the original and the dismantled 3G+C antenna (right).

2.3 The UAV platform

The UAV platform is the construction kit 'Mikrokopter Okto Xl', sold by the company HiSystems GmbH (HISYSTEMS 2013). In order to place the georeferencing sensors of the *PO*-board on the UAV some modifications were necessary: (1) To stabilize the system and to reduce the influence of vibrations the original centerplates, which hold the frame together, were replaced by 2 mm CFK plates. (2) Two of the motor side arms were turned over to be able to mount the ANN-MS antenna on the top of the outer end of one of the arms. (3) A shelf was added in the middle of the frame to provide space for the onboard processing units and two lithium-polymer batteries. The modified UAV is presented in figure 3.

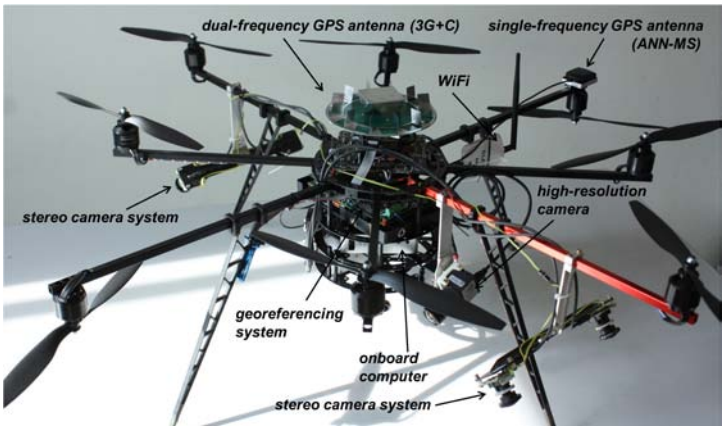

Fig. 3: The modified UAV with all sensor and processing components.

Additionally to the direct georeferencing system, the UAV is also equipped with two stereo camera systems (iDS uEye UI-1221LE, 10Hz), one high-resolution camera (iDS uEye UI-

2280SE, 1Hz), one computer (Zotac Zbox nano) and a Wi-Fi module. The stereo cameras will be used for obstacle detection and visual odometry in further developments. The high-resolution camera is intended to act as mapping sensor and the computer is used for the image processing and data storage.

The total weight of the UAV platform is 4.8 kg. Therefore, it complies with the German law formalities (weight limit: 5 kg).

2 The RTK-GPS algorithm

In this section the implemented RTK-GPS algorithm is presented. Even if this algorithm is not the final version of the envisaged development, which will include other sensors and advanced motion models, it demonstrates, how the basic RTK-GPS functionality is realized on the onboard real-time processing unit.

2.1 The observables

The GPS provides two types of observations that are generally the basis for GPS positioning. These observation types are the code pseudoranges and the carrier phases. Solutions based on phase ranges are far more accurate than solutions based on code pseudoranges. That is the reason why carrier phases are used as main observations in case of RTK-GPS. Referring to (HOFMANN-WELLENHOF ET AL. 2008) the mathematical model for carrier phase measurements is given by

$$\Phi_A^j(t) = \frac{1}{\lambda}\rho_A^j(t) + N_A^j + \frac{c}{\lambda}\Delta\delta_A^j(t) + \frac{1}{\lambda}\varsigma_A^j + \varepsilon_A^j, \tag{1}$$

where $\Phi_A^j(t)$ is the carrier phase from the satellite *j*, measured at the receiver *A* at the time *t*, expressed in cycles. λ is the wavelength. $\rho_A^j(t)$ is the geometric range and N_A^j is the time independent ambiguity that is inherently integer. $\Delta\delta_A^j$ is the combined satellite and receiver clock bias and *c* is the speed of light. Finally, the term ς_A^j includes all the remaining range biases, such as the atmospheric refractions. The term ε_A^j denotes the measurement noise.

RTK-GPS is a relative positioning procedure. This means that the unknown coordinates of a moveable rover station are determined with respect to a stationary master station. The advantage of this relative positioning is an improved accuracy that comes from single- and double-differencing the observations. Due to the single-differencing the satellite clock bias as well as the atmosphere refractions can be reduced significantly, where the order of the reduction is mainly dependent on the baseline length. Due to the double-differencing also the influence of the receiver clock bias is eliminated. The mathematical model of a short-baseline double-difference (DD) carrier phase measurement is given by

$$\Phi_{RM}^{jk}(t) = \frac{1}{\lambda}\rho_{RM}^{jk}(t) + (N_{RM}^j - N_{RM}^k) + \varepsilon_{RM}^{jk}\,. \tag{2}$$

$\Phi_{RM}^{jk}(t)$ is the DD phase range. N_{RM}^j and N_{RM}^k are the single difference (SD) ambiguities. To simplify matters the terms of the remaining systematic errors are neglected in this equation.

The double-differencing can also be done for code pseudoranges:

$$P_{RM}^{jk}(t) = \rho_{RM}^{jk}(t) + \varepsilon_{RM}^{jk} \,. \tag{3}$$

Thus, the DD code pseudorange $P_{RM}^{jk}(t)$ is represented by the geometric range DD $\rho_{RM}^{jk}(t)$ and a noise term.

The aim of the RTK-GPS processing is the determination of the rover position $\boldsymbol{r_R} = [r_{R,x}, r_{R,y}, r_{R,z}]^T$ relative to the master position. However, the inherently unknown DD ambiguities $N_{RM}^{jk} = N_{RM}^{j} - N_{RM}^{k}$ first have to be fixed to integer values in the ambiguity estimation process to allow for a cm-accurate positioning.

2.2 The parameter estimation

The parameter estimation is performed in three steps: (1) float solution, (2) integer ambiguity estimation and (3) fixed solution.
The float solution is the step, where the ambiguities are estimated as real numbers. This estimation can be realized using a least-squares adjustment (LSA) or a Kalman filter. For example in (ODIJK ET AL. 2007) it was shown that Kalman filtering may also lead to a reliable ambiguity resolution, if only single frequency observations are available. This is the same for dual-frequency GPS in case of poor measurement conditions. The advantage of a Kalman filter is that the estimated float ambiguity parameters improve over time. This effect increases, when the dynamic model of the UAV is a priori known or if additional sensors are integrated. Currently, the authors are working towards a tightly-coupled integration of the IMU sensors in the algorithm. In the current state of the implementation a simple random walk model is assumed to proof the functionality of the RTK-GPS algorithm. Even if this is a simple model, it agrees with the movement of every vehicle, when the process noise is chosen appropriate.

Beside the rover position the Kalman filter state vector $\boldsymbol{x_{SD}}$ contains SD ambiguities instead of DD ambiguities. The reason for this is to avoid the hand over problem that would arise for DD ambiguities, when the reference satellite changes (TAKASU & YASUDA 2009).

$$\boldsymbol{x_{SD}} = \left[r_{R,x}\ r_{R,y}\ r_{R,z}\ N_{RM,L1}^{1} \ldots N_{RM,L1}^{n}\ N_{RM,L2}^{1} \ldots N_{RM,L2}^{n}\right]^T \tag{4}$$

To allow for an instantaneous ambiguity resolution the observation vector $\boldsymbol{l}$ consists of DD carrier phases and pseudoranges on the GPS-L1 and the GPS-L2 frequency.

$$\boldsymbol{l} = \left[\Phi_{RM.L1}^{1k} \ldots \Phi_{RM,L1}^{mk}\ \Phi_{RM.L2}^{1k} \ldots \Phi_{RM,L2}^{mk}\ P_{RM,L1}^{1k} \ldots P_{RM,L1}^{mk}\ P_{RM,L2}^{1k} \ldots P_{RM,L2}^{mk}\right]^T \tag{5}$$

The prediction step of the extended Kalman filter calculation is as follows:

$$\begin{aligned} \hat{\boldsymbol{x}}_{\boldsymbol{SD}}(t_{k+1}, t_k) &= \boldsymbol{T}(t_{k+1}, t_k) \cdot \hat{\boldsymbol{x}}_{SD}(t_k) \\ \textstyle\sum_{\hat{x}_{SD}}(t_{k+1}, t_k) &= \boldsymbol{T}(t_{k+1}, t_k) \cdot \textstyle\sum_{\hat{x}_{SD}}(t_k) \cdot \boldsymbol{T}(t_{k+1}, t_k)^T + \boldsymbol{Q}(t_k) \end{aligned} \tag{6}$$

Since the system equation is currently chosen as a random walk model, the transition matrix $\boldsymbol{T}$ is an identity matrix. $\boldsymbol{Q}$ is the process noise matrix. Further information to the choice of the process noise is included later in this section.

The update step includes the equations (7)-(8):

$$\begin{aligned} \hat{\boldsymbol{x}}_{SD}(t_{k+1}) &= \hat{\boldsymbol{x}}_{SD}(t_{k+1},t_k) + \boldsymbol{K}(t_{k+1})\cdot\boldsymbol{d}(t_{k+1}) \\ \textstyle\sum_{\hat{x}_{SD}}(t_{k+1}) &= (\boldsymbol{I}-\boldsymbol{K}(t_{k+1})\cdot\boldsymbol{H}(t_{k+1}))\cdot\textstyle\sum_{\hat{x}_{SD}}(t_{k+1},t_k) \qquad \text{where} \end{aligned} \tag{7}$$

$$\begin{aligned} \boldsymbol{d}(t_{k+1}) &= \boldsymbol{l}(t_{k+1}) - \boldsymbol{H}(t_{k+1})\cdot\hat{\boldsymbol{x}}_{\boldsymbol{SD}}(t_{k+1},t_k) \qquad \boldsymbol{K}(t_{k+1}) = \textstyle\sum_{\hat{x}_{SD}}(t_{k+1},t_k)\cdot\boldsymbol{H}(t_{k+1})^T\cdot\textstyle\sum_{\boldsymbol{d}}(t_{k+1})^{-1} \\ \textstyle\sum_{\boldsymbol{d}}(t_{k+1}) &= \textstyle\sum_{\boldsymbol{l}}(t_{k+1}) + \boldsymbol{H}(t_{k+1})\cdot\textstyle\sum_{\hat{x}_{SD}}(t_{k+1},t_k)\cdot\boldsymbol{H}(t_{k+1})^T \end{aligned} \tag{8}$$

The matrix $\boldsymbol{K}$ is the Kalman gain matrix and the vector $\boldsymbol{d}$ the innovation. The design matrix $\boldsymbol{H}$ represents the nonlinear functional model for a single baseline (one master, one rover).

$$\boldsymbol{H}(t_{k+1}) = \begin{bmatrix} \boldsymbol{A} & \lambda_{L1}\boldsymbol{D_{L1}} & 0 \\ \boldsymbol{A} & 0 & \lambda_{L2}\boldsymbol{D_{L2}} \\ \boldsymbol{A} & 0 & 0 \\ \boldsymbol{A} & 0 & 0 \end{bmatrix}, \quad \boldsymbol{D_{L1,2}} = \begin{bmatrix} 1 & -1 & \\ \vdots & & \ddots \\ 1 & & & -1 \end{bmatrix} \tag{9}$$

The $\boldsymbol{D}$ matrix is the double differencing matrix. Generally, the $\boldsymbol{D}$ matrix is different for the L1 and the L2 observations, since in dynamic applications L1 signals are often more available than L2 signals. The matrix $\boldsymbol{A}$ consist of the differences of the line of sight vectors from the predicted rover position to the satellites *m* and *k* (e.g. HOFMANN-WELLENHOF ET AL. 2008). The Covariance matrix $\textstyle\sum_{\boldsymbol{l}}(t_{k+1})$ includes the measurement noise.

For a successful ambiguity resolution the measurement and the process noise of the implemented extended Kalman filter have to be selected carefully. The experience of the authors is that the following settings lead to the best results for the presented filter type.

Measurement noise:
Since the pseudoranges are less accurate than the carrier phases, a distinction must be made between the carrier phase measurement noise σ_ϕ and the pseudorange measurement noise σ_P, using a factor of *f=100*. Thus, the SD measurement noise is set to:

$$\sigma_\phi^2 = 2\cdot\left(a^2 + (b/\sin el)^2\right) \text{ and } \sigma_P^2 = 2\cdot\left(a^2\cdot f^2 + (b/\sin el)^2\cdot f^2\right) \tag{10}$$

Tests with single- and dual-frequency data have shown that the elevation independent parameter *a* can be set to zero, whereas the elevation dependent parameter *b* should not be omitted. The author's experience is that *a=2 mm* and *b=2 mm* lead to the best results. In the resulting covariance matrix $\textstyle\sum_{\boldsymbol{l}}$ also DD correlations are regarded.

$$\begin{aligned} \boldsymbol{R}_\phi &= diag\left(\sigma_{\phi,L1}^{1\,2}\ldots\sigma_{\phi,L1}^{m\,2}\,\sigma_{\phi,L2}^{1\,2}\ldots\sigma_{\phi,L2}^{m\,2}\right) \\ \boldsymbol{R}_P &= diag\left(\sigma_{P,L1}^{1\,2}\ldots\sigma_{P,L1}^{m\,2}\,\sigma_{P,L2}^{1\,2}\ldots\sigma_{P,L2}^{m\,2}\right) \end{aligned}, \qquad \textstyle\sum_{\boldsymbol{l}} = \begin{bmatrix} \boldsymbol{D}\,\boldsymbol{R}_\phi\,\boldsymbol{D}^T & 0 \\ 0 & \boldsymbol{D}\,\boldsymbol{R}_P\,\boldsymbol{D}^T \end{bmatrix} \tag{11}$$

Process noise:
The process noise matrix is a diagonal matrix consisting of two types of process noise. Since the filter is mainly focused on estimating the ambiguities, the process noise for the position parameters is set to σ_{pos}*=1m*. This choice reflects the approximate dynamic capabilities of the UAV but doesn't smooth the positions to much. In contrast, the ambiguity parameters are assumed to be constant. Thus, their process noise could generally be set to zero. However, when slight variations of the ambiguity parameters are permitted, the para-

meters react better on changing satellite configurations. This is why the process noise for the ambiguity parameters is set to $\sigma_{amb}=1\cdot10^{-4}$ *cycles*.

$$\boldsymbol{Q} = diag\left(\sigma_{pos}^2\ \sigma_{pos}^2\ \sigma_{pos}^2\ \sigma_{amb,L1}^{1\ 2}\ldots\sigma_{amb,L1}^{n\ 2}\ \sigma_{amb,L2}^{1\ 2}\ldots\sigma_{amb,L2}^{n\ 2}\right) \tag{12}$$

For the initialization of the ambiguity parameters the SD pseudorange - carrier phase difference, divided by the wavelength, is used. Since this initialization is very imprecise, the process noise of new ambiguity parameters is set to a very large value ($\sigma_{amb}=100$ *cycles*) in the first epoch. In this way the new initialized ambiguities don't have any influence on the other parameters, but benefit from the current float solution.

The results of the float solution are real ambiguities and their covariance matrix. In step (2) these results can afterwards be used to fix the ambiguities to integer values. Since the SD ambiguities are estimated using DD observations, the float SD ambiguities do not contain a non integer part so that the ambiguity fixing can directly be done on the SD stage. The authors decided to use the MLAMBDA method (CHANG ET AL. 2005) for the integer ambiguity estimation, since this method is, in comparison to the original LAMBDA method (TEUNISSEN 1995), a little bit faster, if many observations are available. The input for the MLAMBDA method are the SD float ambiguities and their covariance matrix.
Finally, in the validation step a decision must be made, if the result of the ambiguity search can be accepted. This is done by the simple ratio test (VERHAGEN & TEUNISSEN 2006), where the squared norm of the ambiguity residuals of the best set of ambiguities (R_1) and the second best set of ambiguities (R_2) is compared. Only if the quotient R_2/R_1 exceeds a threshold of 3 the SD ambiguities can be fixed to integer values. Once the ambiguity resolution has been successful the fixed solution follows, where the final baseline parameters are estimated. In a tightly-coupled approach this would also be computed in a filter. In the current implementation a LSA is used. Here, the integer DD ambiguities $\breve{\boldsymbol{N}}_{\boldsymbol{DD}}$, which can be computed from the fixed SD ambiguities $\breve{\boldsymbol{N}}_{\boldsymbol{SD}}$ using equation (13), are directly added to the DD carrier phase observations.

$$\breve{\boldsymbol{N}}_{\boldsymbol{DD}} = \begin{bmatrix} \boldsymbol{D}_{L1} & \boldsymbol{0} \\ \boldsymbol{0} & \boldsymbol{D}_{L2} \end{bmatrix} \cdot \breve{\boldsymbol{N}}_{\boldsymbol{SD}}, \text{ where } \breve{\boldsymbol{N}}_{\boldsymbol{SD}} = \left[\breve{N}_{RM,L1}^{1}\ldots\breve{N}_{RM,L1}^{n}\ \breve{N}_{RM,L2}^{1}\ldots\breve{N}_{RM,L2}^{n}\right] \tag{13}$$

In the current implementation only the entire ambiguity vector is fixed, since this is, in the first instance, the most reliable solution. Of course, in case the resolution of the entire SD ambiguity vector fails, also a subset of the ambiguity vectors (e.g. excluding low elevation satellites) could be considered. Such implementations are planned for the future, when the IMU observations are integrated in the Kalman filter algorithm.

A special challenge in the described system is the handling of the master observations. As already mentioned in section 2.1, the data connection between the master station and the *PO*-board is realized by two 868 MHz radio modules. However, radio connections like this are in general not fast and reliable enough, to send master observations with a rate of 10 Hz, which is the RTK-GPS processing rate. Even if the data is sent with a rate of 1 Hz, the packets generally arrive with a delay or are lost completely in some conditions (e.g., when the signal path is blocked by a large building). On this account an extrapolation from the last receive time to the current RTK-GPS processing time is needed for the master observations. This extrapolation is realized by a simulation of the master observations (see figure

4), which is based on the fixed and known master antenna coordinates, the satellite broadcast ephemeris as well as the time for which the simulation is applied (MOHINO ET AL. 2005). The idea is that not the real master observations but the current simulation error is the input for the RTK-GPS processing. This simulation error is determined in the master task, every time when new master signals are received at the *PO*-board. In the rover task, which is running with a rate of 10 Hz, the master observations are also simulated, but for the current rover observation time (t_R), and updated with the latest simulation error, assuming that this error keeps constant over a short time. In this way, interruptions of the connection can even be bridged for up to 30 s with a position drift of mostly less than 10 cm.

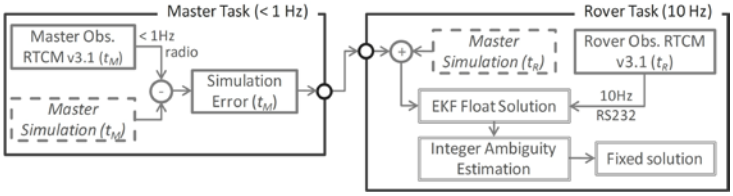

Fig. 4: The task scheduling of the RTK-GPS software on the *PO*-board.

2.3 Cycle Slip detection

Usually, the time to fix the ambiguities with the algorithm described above takes a few epochs, but often the ambiguities can already be fixed within the first epoch. Once the ambiguities are resolved successfully, they can be held fixed, as long as no signal interruption or cycle slip occurs. Thus, a reliable cycle slip detection is required for that. In the current implementation the geometry free L1 and L2 carrier phase linear combination and the receiver lock time indicator are used to detect cycle slips. However, it is well known that the geometry free linear combination is only applicable, when L1 and L2 signals can be observed, and is not able to detect all combinations of cycle slips (BISNATH 2000). Therefore, the authors are currently working on improving the cycle slip detection using IMU data.

4 Results of a test flight

To show that the direct georeferencing system is working well on the presented UAV platform the results of a test flight will be shown in this section (see figure 5).

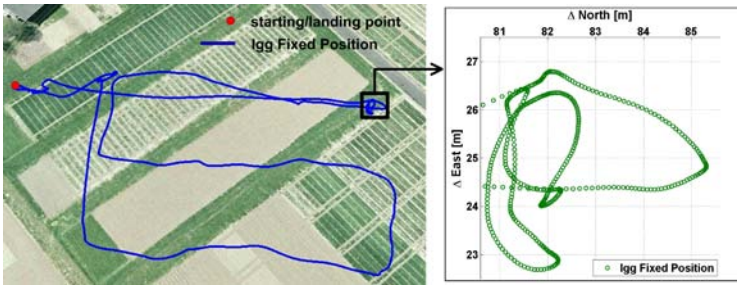

Fig. 5: The RTK-GPS positions, which were determined by the *PO*-board (IGG) in real-time during a test flight in Bonn.

During the flight the real-time processed positions and the GPS raw observations were logged on the *PO*-board. Afterwards, the real-time positions of the *PO*-board, determined using the presented RTK-GPS algorithm, which is abbreviated with IGG in the following text, could be compared to the results of different GNSS software packages, such as RTKLIB (TAKASU & YASUDA 2009) and Leica Geo Office (LGO) (LEICA 2013). In figure 6 the differences of the IGG height component to the results of the other software packages are presented. In this figure it becomes apparent that: (1) The IGG-LGO time series contains much less values than the IGG-RTKLIB time series. This effect is caused by the different sampling rates of the master (1Hz) and the rover (10Hz). While the RTKLIB and the in-house developed IGG software can deal with these different sampling rates LGO only provides results for the epochs where rover and master observations are available. (2) In the IGG-RTKLIB time series a distinction is made between fixed and float solutions. The reason is that the RTKLIB only provided float solutions in a few epochs. (3) The IGG-RTKLIB and the IGG-LGO differences are mostly less than 5 mm, but sometimes larger differences occur. The reason for this effect is that due to the radio connection the data of the master station has not always been available on time in the real-time processing, where the maximum time lag was 2.5 sec in this test. In contrast, for the post processing, the master data was always available on time. Thus, there were different observables used in the real-time and in the postprocessing so that the influence of the time lags of the master data is getting visible. These differences are always in the level of the accuracy of RTK-GPS.

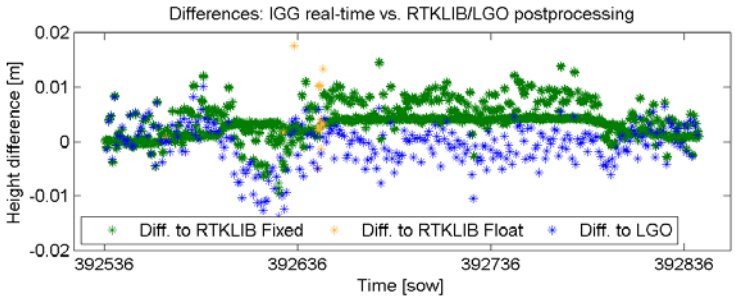

Fig. 6: Differences of the heights that were determined by the *PO*-board in real-time (IGG) and the heights that were determined in the post processing (RTKLIB, LGO) .

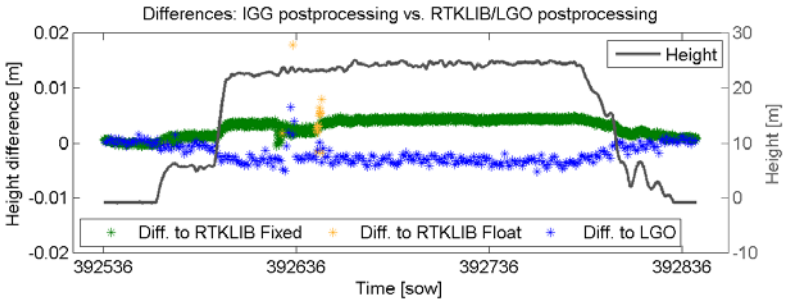

Fig. 7: Differences of the IGG postprocessing heights to the postprocessing results of RTKLIB and LGO as well as the UAV heights relative to the master station.

In order to clarify that these larger differences really arise from the transmission times of the master data, the logged raw data was also processed with the IGG post processing software. In this software the same algorithm is used as on the *PO*-board, but in contrast the master observations are available without a delay. In figure 7 the differences of the IGG postprocessing results to the results of the other software packages are shown. Compared to the results from figure 6, the large differences are no longer visible, confirming the assumption that the differences arise from the transmission delay. However, in figure 7 it can be seen that the IGG-RTKLIB height differences are mostly positive while the IGG-LGO height differences are mostly negative. The reason for this is that different troposphere models are used in the different software packages (in the IGG software a modified Hopfield model (GOAD & GOODMAN 1974) is used). Thus, depending on the flight altitude differences in the troposphere modeling become visible in the height component, whereas the solution of the in-house developed software lies between the results of the other software packages. In the north and in the east components these differences are not visible. There the maximum differences are less than 1 mm for the complete time series.

5 Conclusion and outlook

In this contribution the current state of the development of a direct georeferencing system has been presented. In this context the reasons for implementing an own RTK-GPS software as well as details to the first version of the RTK-GPS algorithm have been discussed. Results of a flight test have shown that the system is already applicable on lightweight UAVs. Thus, the groundwork for further developments and improvements is laid. Planned developments are:

(a) Due to the integration of IMU observations in the process model of the Kalman filter the RTK-GPS float solution can be improved. In doing so not only the time to fix the ambiguities will decrease, but this will also allow for a more robust cycle slip detection.

(b) The authors are currently working towards the integration of the single-frequency GPS baseline in the attitude determination. The GPS attitude determination will be done in a tightly coupled approach, where the observations of the accelerometers, gyroscopes and the magnetometers are involved.

(c) The four cameras on the UAV, used for visual odometry calculation (SCHNEIDER ET AL. 2013), will also be integrated in the GPS algorithms. The final position determination will then be realized in a superior filter fusing the GPS, IMU and visual observations.

(d) The system still has to be calibrated (boresight and lever-arm calibration). Furthermore, the results of the system have to be evaluated. The evaluation can for example be done tracking the UAV with a video tachymeter during a flight.

Acknowledgement

The authors wish to express their gratitude to the DFG (Deutsche Forschungsgemeinschaft) for supporting this work in the context of the project "Mapping on Demand" (project number FOR 1505).

References

BISNATH, S. B. (2000): Efficient, automated cycle-slip correction of dual-frequency kinematic GPS data. In: ION GPS 2000, Salt Lake City, Utah, pp 145-154

BLÁHA, M., EISENBEISS, H., GRIMM, D. & LIMPACH, P. (2011): Direct georeferencing of UAVs. In: UAV-g 2011 conference, Zurich, Switzerland

CHANG, X.-W., YANG, X. & ZHOU, T. (2005): MLAMBDA: A modified LAMBDA method for integer least squares estimation. J Geodesy, Vol. 79, pp 552-565

D'OLEIRE-OLTMANNS, S., MARZOLFF, I., PETER, K.D. & RIES, J.B. (2012): Unmanned aerial vehicle (UAV) for monitoring soil erosion in morocco. Remote Sens. (4), pp 3390-3416

EISSENBEIß, H. (2009): UAV Photogrammetry. Dissertation, ETH Zurich No. 18515

ELING, C., KLINGBEIL, L., WIELAND, M. & KUHLMANN, H. (2013a): A precise position and attitude determination system for lightweight aerial vehicles. UAV-g 2013, Rostock, Germany

ELING, C., ZEIMETZ, P. & KUHLMANN, H. (2013b): Development of an instantaneous GNSS/MEMS attitude determination system. GPS Solut 17, pp 129-138

GOAD, C.C. & GOODMAN, L. (1974): A modified Hopfield tropospheric refraction correction model. Fall Annual Meeting of the American Geophysical Union, San Francisco

HISYSTEMS (2013): HiSystems GmbH, the mikrokopter shop: www. mikrokontroller.com

HOFMANN-WELLENHOF, B., LICHTENEGGER, H. & WASLE, E. (2008): GNSS Global Navigation Satellite Systems. Springer-Verlag Wien New York, ISBN 978-3-211-73012-6

LEICA (2013): Leica Geosystems - Leica Geo Office, url: http://www.leica-geosystems.de/de/Leica-Geo-Office_4611.htm

MOHINO, E., GENDE, M., BRUNINI, C. & HERAIZ, M. (2005): Sigog: simulated gps observation generator. GPS Solut 9, pp 250-254

MORALES, Y. & TSUBOUCHI, T. (2007): DGPS, RTK-GPS and Starfire DGPS performance under tree shading environments. In: IEEE Int. Conf. on Integration Technology, Shenzhen, China

NAGAI, M., CHEN, T., SHIBASAKI, R., KUMAGAI, H. & AHMED, A. (2009): UAV-borne 3-D mapping system by multisensor integration. IEEE T Geosci Remote 47(3), pp 701-708

ODIJK, D., TRAUGOTT, J., DACHS, G., MONTENBRUCK, O. & TIBERIUS, C. (2007): Two precision GPS approaches applied to kinematic raw measurements of miniaturized L1 receivers. In: ION GPS-2007, Institute of Navigation (ION), Manassas, VA

SCHNEIDER, J., LÄBE, T. & FÖRSTNER, W. (2013): Incremental real-time bundle adjustment for multi-camera systems with points at infinity. UAV-g 2013, Rostock, Germany

ŠKALOUD, J. (1999): Optimizing Georeferencing of Airborne Survey Systems by INS/DGPS. PhD thesis, University of Calgary

TAKASU, T. & YASUDA, A. (2009): Development of the low-cost RTK-GPS receiver with an open source program package RTKLIB. Intern. Symp. on GPS/GNSS 2009, ICC Jeju, Korea

TEUNISSEN, P.J.G. (1995): The least-squares ambiguity decorrelation adjustment: a method for fast GPS integer ambiguity estimation. J Geodesy, Vol. 70, pp 65-82

VERHAGEN, S. & TEUNISSEN, P.J.G. (2006): New Global Navigation Satellite System Ambiguity Resolution Method Compared to Existing Approaches. J Guid Control Dynam, Vol. 29, No 4, pp 981-991

ZEIMETZ, P. & KUHLMANN, H. (2010): Validation of the laboratory calibration of geodetic antennae based gps measurements, in: FIG Working Week, Sydney, Australia